Critical end point behavior in a binary fluid mixture

Nigel B. Wilding*

Institut für Physik, Johannes Gutenberg Universität, Staudinger Weg 7, D-55 099 Mainz, Germany

(Received 10 December 1996)

We consider the liquid-gas phase boundary in a binary fluid mixture near its critical end point. Using general scaling arguments, we show that the diameter of the liquid-gas coexistence curve exhibits singular behavior as the critical end point is approached. This prediction is tested by means of extensive Monte Carlo simulations of a symmetrical Lennard-Jones binary mixture within the grand canonical ensemble. The simulation results show clear evidence for the proposed singularity, as well as confirming a previously predicted singularity in the coexistence chemical potential [M. E. Fisher and P. J. Upton, Phys. Rev. Lett. **65**, 2402 (1990)]. The results suggest that the observed singularities, particularly that in the coexistence diameter, should also be detectable experimentally. [S1063-651X(97)04706-5]

I. INTRODUCTION

A critical end point occurs when a line of second-order phase transitions intersects and is truncated by a first-order phase boundary, beyond which a new *noncritical* phase is formed. Critical end points are common features in the phase diagrams of a many multicomponent systems such as binary fluid mixtures, binary alloys, and liquid crystals. They also occur under certain circumstances in pure systems having additional internal degrees of freedom such as superfluids, as well as certain ferromagnets and ferroelectrics.

Perhaps the simplest system to exhibit a critical end point is a binary fluid mixture. Here the phase diagram is spanned by three thermodynamic fields: the temperature T, a chemical potential μ, and an ordering field h coupling to the concentration difference of the two particle species. A number of different phase diagram topologies are possible for binary fluids depending on the microscopic interaction parameters, as systematically classified by Konynenburg and Scott [1]. The particular case on which we shall focus in this work is of type II in their classification scheme and is depicted schematically in Fig. 1 for the subspace $h=0$. Within this subspace, two fluid phases β and γ, each rich in one of the two particle species, coexist with one another. By tuning T and μ, however, one finds a critical λ line $T_c(\mu)$, where both phases merge into a single disordered $\beta\gamma$ phase. The point at which the λ line $T_c(\mu)$ intersects the first-order line of liquid-gas transitions $\mu_\sigma(T)$ marks the critical end point (T_e, μ_e). For $T<T_e$, the phase boundary $\mu_\sigma(T)$ constitutes a triple line along which the fluid phases β and γ coexist with the gas phase α, while for $T>T_e$, $\mu_\sigma(T)$ defines the region where the $\beta\gamma$ and α phases coexist. Precisely at the critical end point the critical mixture of β and γ phases coexists with the gas phase. Since the gas phase does not participate in the criticality, it is commonly referred to as a ''spectator'' phase.

Interest in critical end points has recently been aroused following theoretical work by Fisher and co-workers [2]. On the basis of phenomenological scaling and thermodynamic arguments, these authors argued that the nonanalytic behavior at the critical end point engenders a free-energy-like singularity in the first-order (spectator) phase boundary $\mu_\sigma(T)$. The nature of this singularity, specifically its amplitude ratio, was related to the universal features of the critical line. Additionally, different universal amplitude ratios were proposed for the noncritical surface tensions near the critical end point [3]. These predictions were subsequently corroborated by analytical calculations on extended spherical models [4,5], as well as a Landau theory study of a model ferroelectric [6]. To date, however, experimental results pertaining to critical end points are scarce and those that do exist have focused on the interfacial properties and the surface amplitude ratios [7,8]. To the best of our knowledge there have been no reported attempts to study the bulk coexistence properties and the matter of the predicted singularity in the
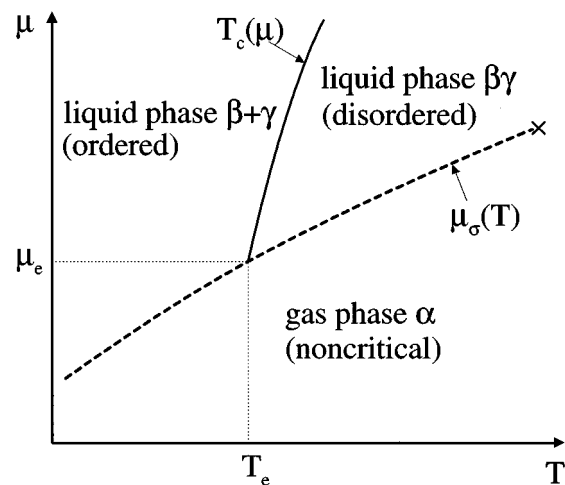

FIG. 1. Schematic phase diagram of a binary fluid in the coexistence surface $h=0$. The broken line $\mu_\sigma(T)$ is the first-order liquid-gas phase boundary between the fluid and gas phase α. The full line is the critical line of second-order transitions $T_\lambda(\mu)$ separating the demixed phases $\beta+\gamma$ from the mixed phase $\beta\gamma$. The two lines intersect at the critical end point.

————
*Present address: Department of Physics and Astronomy, The University of Edinburgh, West Mains Road, Edinburgh EH9 3JZ, United Kingdom.

spectator phase boundary. There is a similar dearth of simulation work on the subject, and we know of no detailed numerical studies of critical end point behavior, in either lattice or continuum models.

In this paper we address the issue of the nature of the spectator phase boundary near a critical end point by means of computer simulation of a continuum binary fluid model [9]. Our paper is organized as follows. In Sec. II we briefly review the principal features of the scaling arguments of Fisher and co-workers and show that in addition to the previously predicted singularity in $\mu_\sigma(T)$, they also imply singular behavior in the *diameter* of the liquid-gas coexistence curve at the critical end point. In Sec. III we detail extensive Monte Carlo simulations of a symmetrical (Lennard-Jones) binary fluid mixture. We map the liquid-vapor coexistence curve and the λ line of the model by applying finite-size scaling analyses to the probability distribution functions of appropriate observables. The results provide remarkably clear signatures of divergences in the appropriate temperature derivatives of the coexistence diameter and the phase boundary chemical potential, thus corroborating the theoretical predictions. Finally, in Sec. IV we detail our conclusions.

II. THE LIQUID-GAS COEXISTENCE CURVE

A. The coexistence chemical potential

In this subsection we briefly review the scaling arguments of Fisher and Barbosa [2] concerning the singularity in the spectator phase boundary at the critical end point. In so doing, we shall continue to employ the language of the binary fluid mixture, although the arguments themselves are not restricted to this case.

Within the grand canonical framework, liquid-gas coexistence is prescribed by the equality of the Gibbs free energy $G = -k_B T \ln \mathcal{Z}$ in the respective phases, i.e.,

$$G_g(\mu_\sigma(T), T, h) = G_l(\mu_\sigma(T), T, h). \quad (2.1)$$

Since the gas spectator phase is necessarily noncritical, its free energy is analytic at the end point and can thus be expanded as

$$G_g(\mu, T, h) = G_e + G_1^g \Delta\mu + G_2^g t + G_3^g h + G_4^g \Delta\mu^2 + \cdots, \quad (2.2)$$

where $t \equiv T - T_e$ and $\Delta\mu \equiv \mu - \mu_e$, with $\Delta\mu < 0$.

The liquid phase, on the other hand, is critical and therefore contains both an analytic (background) and a *singular* contribution to the free energy

$$G_l(\mu, T, h) = G_0(\mu, T, h) - |\tau|^{2-\alpha} \mathcal{G}_\pm(\hat{h}|\tau|^{-\Delta}), \quad (2.3)$$

where G_0 is the analytic part, while $\mathcal{G}^\pm(y)$ is a universal scaling function that is a function of the relevant scaling fields $\tau(T, \mu, h) = T - T_c(\mu)$ and $\hat{h}(T, \mu, h) \approx h$ that measure deviations from the λ line. $\mathcal{G}^\pm(y)$ must satisfy matching conditions as $y \to \pm\infty$, and the quantities α and Δ are, respectively, the specific heat and gap exponents associated with the λ line.

To linear order the scaling fields may be expanded as

$$\tau(T, \mu, h) = t + a_1 h + a_2 \Delta\mu, \quad (2.4a)$$

$$\hat{h}(T, \mu, h) = h + b_1 t + b_2 \Delta\mu, \quad (2.4b)$$

where the a_i and b_i are nonuniversal ''field mixing'' parameters [10,11], some of which have geometrical significance within the phase diagram. In particular, since $\tau = 0$ specifies $T_c(\mu)$, one has at the critical end point

$$a_2 = -\frac{dT_c}{d\mu}, \quad (2.5)$$

representing the gradient of the λ line at the critical end point.

The critical free energy [Eq. (2.3)] can also be expanded in $\Delta\mu$, t, and h. Recalling Eq. (2.2), invoking Eq. (2.1), and solving for $\mu(T)$ then yields [2]

$$\mu_\sigma(T) - \mu_o(T) \approx -X_\pm |t|^{2-\alpha} - Y_\pm |t|^\beta |h| - \frac{1}{2} Z_\pm |t|^{-\gamma} h^2, \quad (2.6)$$

valid as $T \to T_e \pm$, $h \to 0$. Here $X_\pm, Y_\pm, Z_\pm$ are critical amplitudes and α, β, γ are the usual critical exponents characterizing the λ line. Corrections to scaling have been neglected and the background term has the expansion

$$\mu_o(T) = \mu_e + g_1 t + g_2 h + \cdots. \quad (2.7)$$

If we restrict out attention to the coexistence surface $h = 0$ and assume $\alpha > 0$, Eq. (2.6) implies a specific heat-like divergence in the *curvature* of the spectator phase boundary

$$\frac{d^2\mu_\sigma}{dT^2} \approx -\hat{X}_\pm |t|^{-\alpha}, \quad (2.8)$$

where the amplitude ratio $\hat{X}_+/\hat{X}_-$ is expected to be universal [2].

B. The coexistence diameter

Let us now examine the behavior of the coexistence particle number density in the vicinity of the critical end point. Specifically, we shall focus on the coexistence diameter in the region $\hat{h} = 0$, defined by

$$\rho_d(T) \equiv \frac{1}{2}[\rho_g(\mu_\sigma(T)) + \rho_l(\mu_\sigma(T))]. \quad (2.9)$$

The particle density is obtainable from the Gibbs potential as

$$\rho = -\frac{1}{V}\left(\frac{\partial G}{\partial \mu}\right)_{T,h} \quad (2.10)$$

so that

$$\rho_d(T) = -\frac{1}{V}\left(\frac{\partial G_\sigma(\mu_\sigma(T), T)}{\partial \mu}\right)_T \quad (2.11)$$

with

$$G_\sigma(\mu_\sigma(T),T)=[G_g(\mu_\sigma(T),T)+G_l(\mu_\sigma(T),T)]/2. \tag{2.12}$$

Appealing to Eqs. (2.2) and (2.3) and noting that $\beta=2-\alpha-\Delta$ then yields, for the singular behavior

$$\rho_d(T)=U_\pm|\tau(T,\mu_\sigma(T))|^\beta+V_\pm|\tau(T,\mu_\sigma(T))|^{1-\alpha}$$

$$+\text{(terms analytic at } T_e) \tag{2.13}$$

as $\tau\to0$. Here the nonuniversal critical amplitudes take the form

$$U_\pm=b_2\mathcal{G}'_\pm(0), \tag{2.14a}$$

$$V_\pm=a_2(2-\alpha)\mathcal{G}_\pm(0), \tag{2.14b}$$

with $\mathcal{G}'_\pm(z)=d\mathcal{G}_\pm/dz$.

Now, along the liquid-gas coexistence curve, one has, from Eq. (2.4a),

$$|\tau(T,\mu_\sigma(T))|=|t+a_2(\mu_\sigma(T)-\mu_e)|. \tag{2.15}$$

Recalling Eqs. (2.6) and (2.7) (and setting $h=0$), one then finds

$$|\tau(T,\mu_\sigma(T))|=|t|[1+a_2g_1+O(|t|^{1-\alpha})]. \tag{2.16}$$

Thus, to leading order one can write

$$\rho_d(T)=\tilde{U}_\pm|t|^\beta+\tilde{V}_\pm|t|^{1-\alpha}+\text{(terms analytic at } T_e), \tag{2.17}$$

where $\tilde{U}_\pm=(1+a_2g_1)^\beta U_\pm$ and $\tilde{V}_\pm=(1+a_2g_1)^{1-\alpha}V_\pm$. We note that this expression is of the same form as the singularity in the overall density on the λ line [10].

A special case of Eq. (2.17), relevant to the present work, is that for a symmetrical fluid having energetic invariance under $h\to-h$. In this case one finds on symmetry grounds that the field mixing parameters $b_1=b_2=0$ and hence from Eq. (2.14a)

$$\rho_d(T)=\tilde{V}_\pm|t|^{1-\alpha}+\text{(terms analytic at } T_e), \tag{2.18}$$

which implies a divergent diameter derivative

$$\frac{d\rho_d(T)}{dT}\approx\hat{V}_\pm|t|^{-\alpha}, \tag{2.19}$$

where $\hat{V}_\pm=(1-\alpha)\tilde{V}_\pm$. Since this divergence occurs in the first derivative of the observable $\rho_d(T)$, it is in principle more readily visible than that in the second derivative of $\mu_\sigma(T)$; cf. Eq. (2.8). As we shall now show, however, clear signatures of both divergences are readily demonstrable by Monte Carlo simulation.

III. MONTE CARLO SIMULATIONS

A. Model and algorithmic considerations

The simulations described here were performed for a symmetrical binary fluid model using a Metropolis algorithm within the grand canonical ensemble [12]. The fluid is as-

sumed to be contained in volume $V=L^3$ with periodic boundary conditions. The grand canonical partition function takes the form

$$\mathcal{Z}_L=\sum_{N_1=0}^\infty\sum_{N_2=0}^\infty\prod_{i=1}^N\left\{\int d\vec{r}_i\right\}e^{[\mu N-\Phi(\{\vec{r}\})+h(N_1-N_2)]}, \tag{3.1}$$

where $\Phi=\Sigma_{i<j}\phi(r_{ij})$ is the total configurational energy, μ is the chemical potential, and h is the ordering field (all in units of k_BT). $N=N_1+N_2$ is the total number of particles of types 1 and 2.

The interaction potential between particles i and j was assigned the familiar Lennard-Jones (LJ) form

$$\phi(r_{ij})=4\epsilon_{mn}[(\sigma/r_{ij})^{12}-(\sigma/r_{ij})^6], \tag{3.2}$$

where σ is a parameter that serves to set the interaction range, while ϵ_{mn} measures the well depth for interactions between particles of types m and n. In common with most other simulations of Lennard-Jones systems, the potential was truncated at a cutoff radius $r_c=2.5\sigma$ (irrespective of the species of the interacting particles) and left unshifted. To simplify the task of locating interacting particles, a cell decomposition scheme was employed in which the total system volume was partitioned into cubic cells of side r_c. Interactions emanating from a specific particle then extend only as far as the 26 neighboring cells.

An Ising-like symmetry was imposed on the model by choosing $\epsilon_{11}=\epsilon_{22}=\epsilon>0$. This choice endows the system with energetic invariance under $h\to-h$, thereby ensuring that the critical end point lies in the surface $h=0$. We shall accordingly restrict our attention henceforth to this regime. An additional parameter $\epsilon_{12}=\delta$ was used to control interactions between unlike particles. The phase diagram of the model in the surface $h=0$ is then uniquely parametrized by the ratio δ/ϵ. Physically, the role of this ratio in determining the form of the phase diagram can be understood as follows. For $\delta/\epsilon\lesssim1$, the energy penalty associated with contacts between unlike particles is small and hence there is little incentive for phase separation unless the temperature is very low and the density very high. One therefore expects a phase diagram having a critical end point temperature $T_e\ll T_c^{lg}$ and density $\rho_e\gg\rho_c^{lg}$, where T_c^{lg} and ρ_c^{lg} are the liquid-gas critical temperature and density, respectively. Choosing a smaller value of δ/ϵ, however, moves the end point towards the liquid-gas critical point, into which it merges for sufficiently small δ/ϵ, forming a *tricritical point* [13]. Empirically, we find that for $\delta/\epsilon=0.6$, there is a tricritical point, while for $\delta/\epsilon=0.75$ there is a critical end point having $\rho_e\approx2.3\rho_c^{lg}$. The location of the critical end point for larger values of δ/ϵ could not be reliably determined since its density is above that at which the grand canonical particle insertion algorithm (see below) is operable. In this work, all simulations were performed with $\delta/\epsilon=0.7$, which yields critical end point parameters $T_e\approx0.93T_c^{lg}$, $\rho_e\approx1.75\rho_c^{lg}$. This temperature is sufficiently small compared to T_c^{lg} that critical density fluctuations do not obscure the end point behavior, while at the same time ρ_e is not so large as to unduly hinder particle insertions.

In order to sample ergodically the phase space of the model, two sorts of Monte Carlo action are necessary. The first is a particle transfer step in which one attempts either to insert a particle at a randomly chosen position or, alternatively, to delete a randomly chosen existing particle. Candidate particles for insertion are assigned a species type (1 or 2) with equal probability. The second sort of action is an identity swap, in which one chooses an existing particle at random and attempts to change its identity ($1 \rightarrow 2$ or $2 \rightarrow 1$). Combined use of these operations samples the grand canonical ensemble in which the particle density $\rho = N/V$, energy density $u = \Phi/V$, and number difference density $m = (N_1 - N_2)/V$ all fluctuate.

In accordance with convention, we shall employ dimensionless units to express our data:

$$\widetilde{\rho} = \rho\sigma^3, \quad \widetilde{m} = m\sigma^3, \quad \widetilde{u} = u\sigma^3, \tag{3.3}$$

$$\widetilde{T} = k_B T/\epsilon. \tag{3.4}$$

We also note for future reference that our algorithm utilizes not the true chemical potential μ, but an effective chemical potential $\widetilde{\mu}$ to which the true chemical potential is related by

$$\mu = \widetilde{\mu} + \mu_0 - \ln(N/L^3), \tag{3.5}$$

where μ_0 is the chemical potential in the noninteracting (ideal gas) limit. It is this effective value that features in the results that follows.

B. Method and results

In the course of the simulations, three systems sizes of volume $V = (7.5\sigma)^3$, $V = (10\sigma)^3$, and $V = (12.5\sigma)^3$ were studied, corresponding to average particle numbers $N \approx 250$, $N \approx 600$, and $N \approx 1200$, respectively at the critical end point (whose location we discuss below). Following equilibration, runs comprising up to 6×10^9 MCS [14] were performed and the joint distribution $p_L(\widetilde{\rho}, \widetilde{m}, \widetilde{u})$ was sampled approximately every 10^4 MCS and accumulated in the form of a histogram. For each L, simulations were carried out at several (typically five) temperatures along the liquid-gas coexistence curve.

In order to locate the liquid-gas coexistence curve, the finite-size form of the density distribution $p_L(\widetilde{\rho})$ was studied. Precisely at coexistence, $p_L(\widetilde{\rho})$ is (to within corrections exponentially small in L) double peaked with equal weight in both peaks [15]. For a given simulation temperature, this ''equal weight'' criterion can be used to determine the coexistence chemical potential to high accuracy. Close to the liquid-gas critical point, i.e., when $T \lesssim T_c^{lg}$, this task is straightforward; one simple tunes the chemical potential at constant T until the measured form of $p_L(\widetilde{\rho})$ is double peaked. By contrast, however, in the strongly first-order regime ($T \ll T_c^{lg}$), this approach cannot be used to obtain the coexistence form of $p_L(\widetilde{\rho})$ due to the large free-energy barrier separating the coexisting phases. This barrier leads to metastability effects and prohibitively long correlation times. To circumvent this difficulty one must employ advanced sampling schemes. One such scheme is the multicanonical preweighting method [16], which encourages the simulation

to sample the interfacial configurations of intrinsically low probability. This is achieved by incorporating a suitably chosen weight function in the Monte Carlo update probabilities. The weights are subsequently ''folded out'' from the sampled distribution to yield the correct Boltzmann distributed quantities. Use of this method permits the direct measurement of the order-parameter probability distribution at first-order phase transitions, even when the distribution spans many decades of probability.

To fully capitalize on the data gathered in the simulations, the histogram reweighting technique [18] was employed. This technique rests on the observation that histograms accumulated at one set of model parameters can be reweighted to yield estimates of histograms appropriate to another set of not-too-distant parameters. Results from individual simulation runs at different parameters can also be combined in a systematic fashion to provide information over larger regions of the phase diagram. When used in tandem with multicanonical preweighting, the histogram reweighting technique constitutes a powerful tool for mapping the coexistence curve properties of continuum fluid models [17].

Using the multicanonical preweighting technique, simulations of the liquid-gas coexistence curve of the binary fluid were performed. To begin with, the region near the liquid-gas critical point was studied since there the free-energy barrier between the coexisting phases is small and no preweighting function is need. Thereafter, the temperature was reduced in a stepwise fashion and the coexistence form of $p_L(\widetilde{\rho})$ was collected. For each successively lower temperature studied, histogram reweighting was used to obtain a suitable preweighting function by extrapolating from the coexistence histograms previously obtained at higher temperatures. Further details concerning this strategy have been given elsewhere [17]. Figure 2(a) shows the resulting coexistence forms of $p_L(\widetilde{\rho})$ for the system of size $L = 10\sigma$, at a selection of temperatures in the range $0.9\widetilde{T}_C^{lg} < \widetilde{T} < \widetilde{T}_c^{lg}$. Also shown in Fig. 2(b) is the same data expressed on a logarithmic scale. The corresponding estimates for the coexistence chemical potential and the coexistence diameter are plotted in Figs. 3 and 4, respectively. The gas and liquid densities required for the diameter calculation were obtained as the average densities of the respective peaks of $p_L(\widetilde{\rho})$. It is interesting to note from Fig. 2(b) that for the lowest temperature studied ($T \approx 0.9 T_c$), the ratio of minimum to maximum in the distribution is approximately 10^{12}. A free-energy barrier of this magnitude would, of course, represent an insurmountable obstacle to phase-space evolution were it not for the use of multicanonical preweighting.

It is also instructive to examine the coexistence behavior of the number difference order-parameter distribution $p_L(m)$, for temperatures above and below T_e, as shown in Fig. 5. Well below T_e, this distribution is three peaked, with one narrow peak centered on $\widetilde{m} = 0$ and two broader peaks centered on positive and negative values of $\widetilde{m}$. The peak at $\widetilde{m} = 0$ corresponds to the disordered gas phase, while the degenerate peaks at positive and negative values of m represent the ordered A-rich and B-rich liquid phases, respectively. As one approaches the critical end point, however, the liquid peaks become broader and overlap with the gas phase
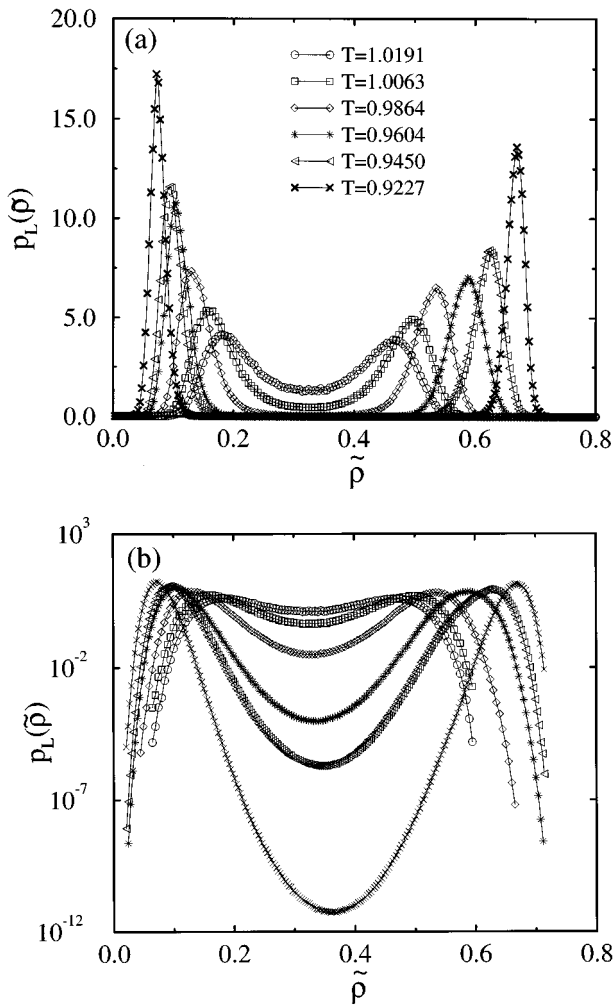
FIG. 2. (a) Estimates of the coexistence density distributions for the $L=10\sigma$ system size, for a range of subcritical temperatures, obtained as described in the text. The lines are merely guides to the eye. Statistical errors do not exceed the symbol sizes. (b) Same data expressed on a logarithmic scale.

peak, ultimately leaving just one single peak at $\widetilde{m}=0$ for $T>T_e$.

To determine the locus of the λ line and the critical end point in which it formally terminates, finite-size scaling (FSS) methods were employed. On the λ line, criticality is signaled by the asymptotic scale invariance of $p_L(\widetilde{m})$. A useful dimensionless measure of the form of this distribution is its fourth-order cumulant ratio $U_L=1-3\langle\widetilde{m}^4\rangle/\langle\widetilde{m}^2\rangle^2$ [19]. If one plots $U_L(\widetilde{T})$ for a given constant $\widetilde{\mu}$, one expects the curves for each L to intersect at the critical demixing temperature. For binary fluids with short-ranged interactions, the critical behavior on the λ line and the critical end point [20] is expected to be Ising-like. One thus expects that asymptotically (for sufficiently large L) there will be a unique crossing point at a universal value U_L^*. Ising model simulations [21] give the estimate $U_L^*=0.470(3)$.

We have measured $U_L(\widetilde{T})$ for several value of the chemical potential $\widetilde{\mu}$, thus enabling an estimate of the locus of the λ line. For each chosen value of $\widetilde{\mu}$, an initial rough estimate of the critical temperature was obtained from a number of
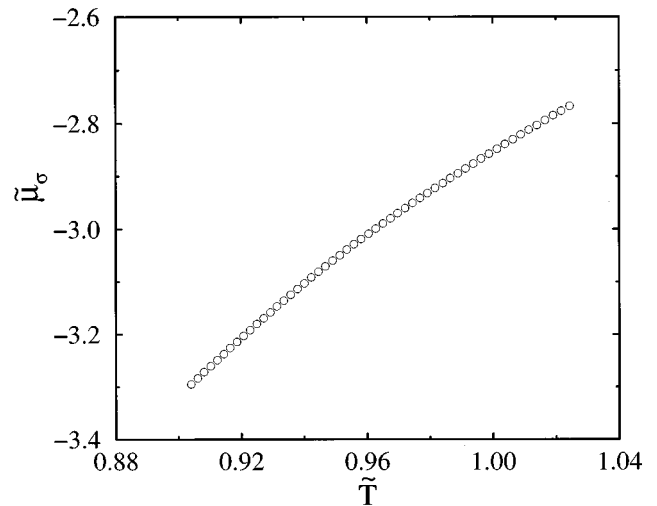

FIG. 3. Temperature dependence of the coexistence chemical potential $\widetilde{\mu}$ obtained from the histogram reweighting of the distributions shown in Fig. 2. Statistical errors do not exceed the symbol sizes.

short simulations, in which the form of $p_L(\widetilde{m})$ was observed visually. Longer runs at this temperature were then carried out for each system size in order to facilitate a more precise determination of $\widetilde{T}_c$. A representative plot of U_L as a function of $\widetilde{T}$ and L is shown in Fig. 6 for the case $\widetilde{\mu}=-2.95$. Each of the curves shown represent the histogram extrapolation of data obtained from a single simulation at the temperature $\widetilde{T}=1.005$. Evidently there is no unique cumulant intersection point for the three system sizes; rather the crossing point for the $L=7.5\sigma$ and $L=10\sigma$ system sizes occurs at larger $\widetilde{T}$ and smaller U_L than for the $L=10\sigma$ and $L=12.5\sigma$ system sizes. It is reasonable to assume, however, that for sufficiently large L, the cumulant intersection point *would* converge on the universal value $U_L^*=0.470(3)$, but that for the system sizes studied here this limit is not attained due to corrections to finite-size scaling and (to a lesser extent) statistical error. In view of this, we adopt as our esti-
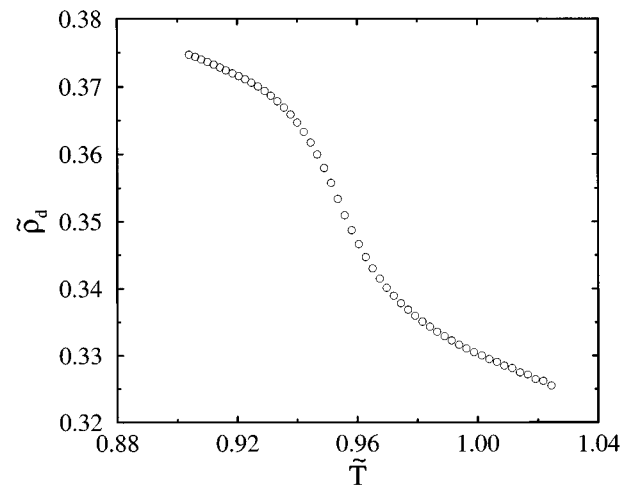

FIG. 4. Temperature dependence of the coexistence curve diameter $\widetilde{\rho}_d=(\widetilde{\rho}_g+\widetilde{\rho}_l)/2$, as obtained from histogram reweighting of the distributions shown in Fig. 2. Statistical errors do not exceed the symbol sizes.

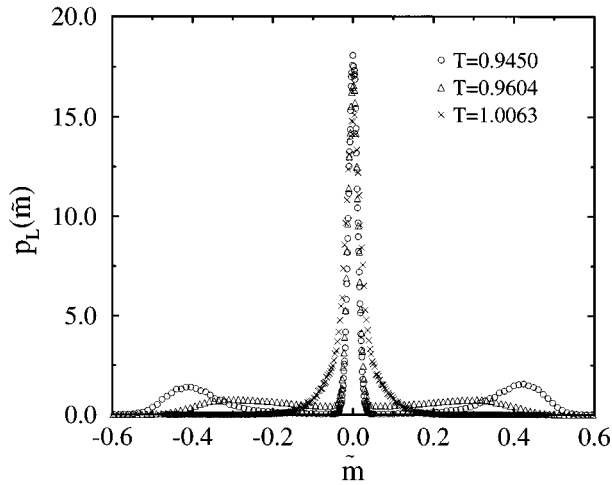FIG. 5. Estimates of the number difference order-parameter distribution $p_L(\widetilde{m})$ for the $L=10\sigma$ system size at three temperatures spanning T_e.

FIG. 6. Measured cumulant ratio $U_L(\widetilde{T})$ for the three system sizes studied. The lines are the results of histogram reweighting of single simulations performed at $\widetilde{T}=1.005$, $\widetilde{\mu}=-2.95$.

mate of $\widetilde{T}_c(\widetilde{\mu})$ that temperature at which the cumulant intersection occurs for the two largest system sizes.

The critical end point was estimated in a similar manner by studying the cumulant ratio U_L for $p_L(\widetilde{m})$ as a function of $\widetilde{T}$ and L along the *liquid* branch of the coexistence curve. In principle, the form of $p_L(\widetilde{m})$ corresponding to the liquid phase can be extracted from the joint coexistence distribution $p_L(\widetilde{\rho},\widetilde{m},\widetilde{u})$ since this embodies contributions from both phases. Assuming there is a clear distinction between the gas and liquid phases (i.e., when $T\ll T_c^{lg}$), one can isolate the liquid branch component simply by disregarding all those histogram entries having $\widetilde{\rho}<\widetilde{\rho}_d$. However, it turns out to be difficult to obtain sufficient statistics for $p_L(\widetilde{m})$ in this way. This is because the preweighted simulation uniformly samples *all* densities between the gas and liquid phases. When the gas and liquid densities are well separated, the simulation spends only a relatively small fraction of the time sampling liquidlike configurations and accordingly the statistical quality of the histogram for $p_L(\widetilde{m})$ is low. To circumvent this problem, it is expedient to perform a simulation that samples *only* the liquid phase while nevertheless remaining at coexistence. This is achievable by setting $\widetilde{T}$ and $\widetilde{\mu}$ to their coexistence values and performing a simulation *without* preweighting the density distribution. If a starting configuration having a liquidlike density is chosen, the simulation will then remain in the liquid phase by virtue of the large free-energy barrier separating it from the gas phase. The results of implementing this procedure are shown in Fig. 7, in which U_L is plotted as a function of temperature along the liquid branch of the coexistence curve in the neighborhood of the critical end point. The curves exhibit an intersection at $\widetilde{T}_e=0.958(2)$, with a cumulant value $U_L=0.47$ for the two largest system sizes and $U_L=0.455$ for the smallest two systems sizes. The associated estimate of the critical end point chemical potential and density are $\widetilde{\mu}_e=-3.017(3)$, $\widetilde{\rho}_e=0.587(5)$.

In the interests of completeness we have also obtained the location of the liquid-gas critical point. This was achieved
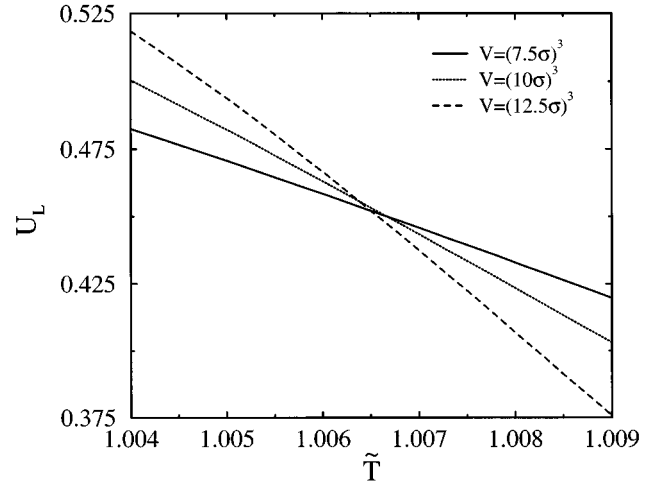
via a FSS study of the densitylike ordering operator. Details of the approach used have been extensively described elsewhere [22,17] and so will not be repeated here. We merely quote the results: $\widetilde{T}_c^{lg}=1.024(2)$, $\widetilde{\rho}_c^{lg}=0.327(2)$, and $\widetilde{\mu}_c^{lg}=-2.767(4)$.

In Fig. 8 we present the estimated phase diagram of our system. Plotted are the coexistence densities for the liquid and gas branches, the position of the liquid-gas critical point, the locus of the λ line, and the position of the critical end point. One observes that close to the liquid-gas critical point, strong finite-size effects occur in the peak densities of $p_L(\widetilde{\rho})$. These have also been observed and discussed in the context of a previous study of the pure LJ fluid [17]. More striking, however, is the appearance of a pronounced "kink" in the liquid branch density close to the critical end point. This is a consequence of the singular behavior on the critical line. As one would expect, the gas branch displays no such kink due to the analyticity of $G_g(\mu,T)$ at T_e.
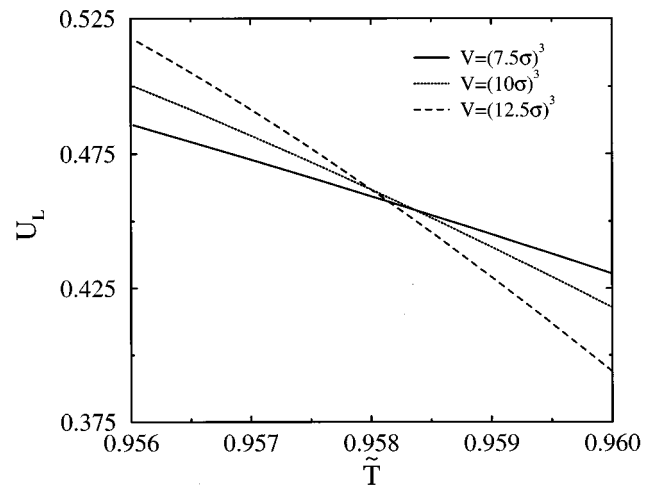

FIG. 7. Cumulant ratio U_L for the distribution $p_L(\widetilde{m})$, obtained according to the procedure described in the text. The lines are the results of histogram reweighting of liquid-phase simulations performed at liquid-gas coexistence.
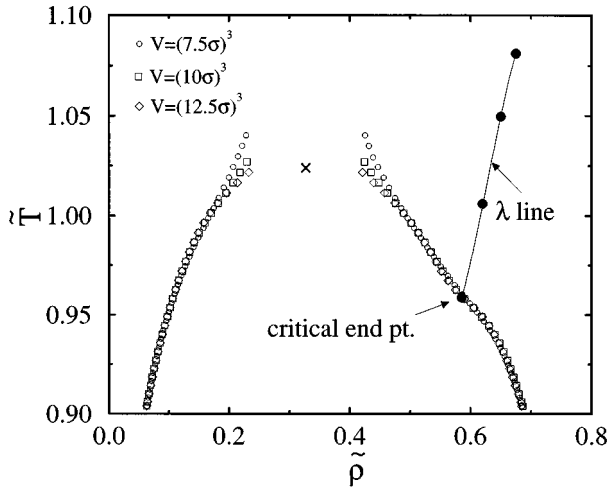
FIG. 8. Average peak densities corresponding to the coexistence form of $p_L(\widetilde{\rho})$ for the three systems sizes studied, plotted as a function of temperature. Also shown is the estimated locus of the λ line (filled circles) and the liquid-gas critical point (cross). Statistical errors do not exceed the symbol sizes.

To probe more closely the behavior of the coexistence density, we plot in Fig. 9(a) the diameter derivative $-d\widetilde{\rho}_d(T)/d\widetilde{T}$, for the three system sizes studied. The data exhibit a clear peak close to T_e, which grows with increasing system size. Very similar behavior is also observed in the curvature of the spectator phase boundary $-d^2\widetilde{\mu}_\sigma/d\widetilde{T}^2$; see Fig. 9(b). These peaks constitute, we believe, the finite-size rounded forms of the divergences [Eqs. (2.19) and (2.8)]. On the basis of finite-size scaling theory [19], the peaks are expected to grow in height like $L^{\alpha/\nu}$, with ν the correlation length exponent. Unfortunately, it is not generally feasible to extract estimates of α/ν in this way (even for simulations of lattice Ising models) because to do so requires the ability to measure the analytic background, for which the present system sizes are much too small. Nevertheless, the correspondence of the peak position with the independently estimated value of $\widetilde{T}_e$, as well as the growth of the peak with increasing L, constitutes strong evidence supporting the existence of the predicted singularities.

IV. DISCUSSION

In summary, we have employed grand canonical Monte Carlo simulations in conjunction with multicanonical preweighting and histogram reweighting to study the first-order phase boundary near the critical end point of a continuum binary fluid model. The results provide clear evidence for the existence of singularities in the phase boundary chemical potential and the coexistence curve diameter. They thus constitute strong corroboration of the scaling arguments on whose basis the singularities are predicted.

Although no experimental observations of singularities at critical end points have yet been reported, we believe that given an appropriately chosen system their presence should be relatively easy to detect. In this respect, a binary fluid model might be a good candidate system for study since, generally speaking, rather precise liquid-gas coexistence
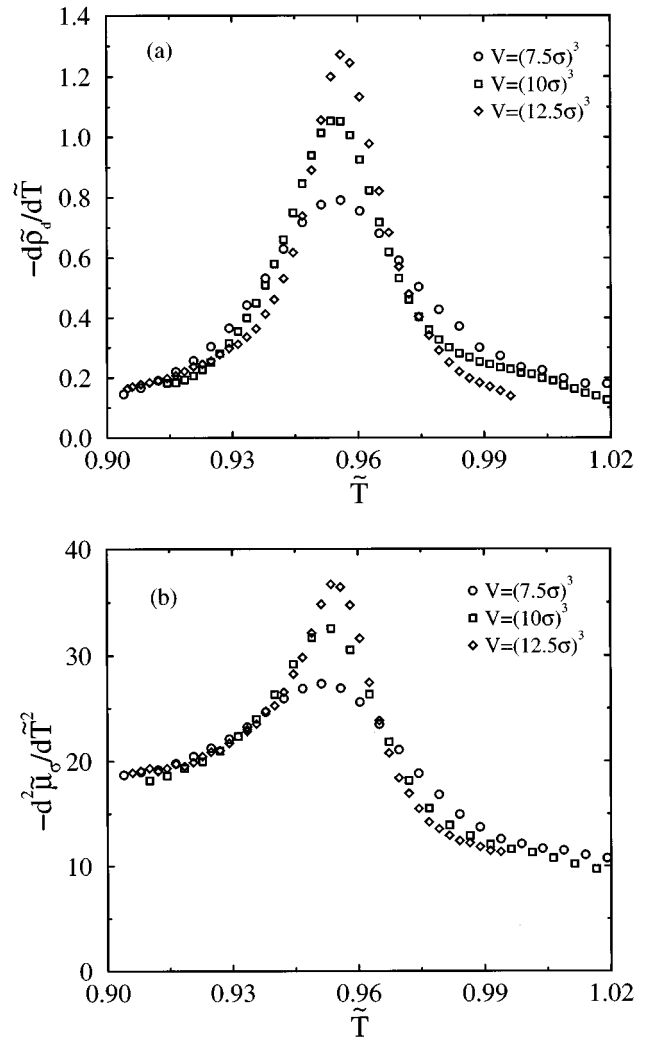

FIG. 9. (a) Numerical temperature derivative of the measured coexistence diameter $-d\rho_d/d\widetilde{T}$ in the vicinity of the critical end point temperature. (b) Measured curvature of the phase boundary $-d^2\widetilde{\mu}_\sigma/d\widetilde{T}^2$ in the vicinity of the critical end point temperature. In both cases data are shown for the three system sizes studied.

curve data can be obtained. In this case the role of the chemical potential in Eq. (2.6) is replaced by the pressure, but otherwise the form of the singularity remains unaltered. Of course, in a real system, the lack of finite-size rounding should render the singularities more conspicuous than in a simulation. Moreover, since real binary fluids do not generally possess a special symmetry between the two fluid components, the chemical potential and temperature feature in the scaling field $\hat{h}$, changing the $|t|^{1-\alpha}$ diameter singularity into a much stronger $|t|^\beta$ singularity (see Sec. II). In future work we also intend to study the consequences of this symmetry breaking via simulations of an asymmetrical binary fluid model.

ACKNOWLEDGMENTS

[1] P.H. van Konynenburg and R.L. Scott, Philos. Trans. R. Soc. Ser. A **298**, 495 (1980).

[2] M.E. Fisher and P.J. Upton, Phys. Rev. Lett. **65**, 2402 (1990); M.E. Fisher and M.C. Barbosa, Phys. Rev. B **43**, 11 177 (1991).

[3] M.E. Fisher and P.J. Upton, Phys. Rev. Lett. **65**, 3405 (1990).

[4] M.C. Barbosa and M.E. Fisher, Phys. Rev. B **43**, 10 635 (1991); M.C. Barbosa, *ibid.* **45**, 5199 (1992).

[5] M.C. Barbosa, Physica A **177**, 153 (1991).

[6] E.L. de Santa Helena and M.C. Barbosa, Physica A **208**, 479 (1994); **219**, 408 (1995).

[7] B.M. Law, Phys. Rev. Lett. **67**, 1555 (1991).

[8] D.S.P. Smith and B.M. Law, J. Chem. Phys. **99**, 9836 (1993).

[9] A brief preliminary report of this work has been given elsewhere: N.B. Wilding, Phys. Rev. Lett. **78**, 1488 (1997).

[10] M.A. Anisimov, E.E. Gorodetskii, V.D. Kulikov, and J.V. Sengers, Phys. Rev. E **51**, 1199 (1995).

[11] J.J. Rehr and N.D. Mermin, Phys. Rev. A **8**, 472 (1973).

[12] M.P. Allen and D.J. Tildesley *Computer Simulation of Liquids* (Oxford University Press, London, 1987).

[13] In general, binary fluids do not exhibit a tricritical point. The appearance of one in this model is traceable to its special symmetry. For a recent simulation study of tricritical behavior in a symmetric continuum fluid model see N.B. Wilding and P. Nielaba, Phys. Rev. E **53**, 926 (1996).

[14] We define a Monte Carlo step (MCS) to comprise a particle transfer attempt (insertion or deletion) *and* a particle identity change (type $1 \rightarrow 2$ or $2 \rightarrow 1$) attempt.

[15] C. Borgs and R. Kotecký, Phys. Rev. Lett. **68**, 1734 (1992).

[16] B. Berg and T. Neuhaus, Phys. Rev. Lett. **68**, 9 (1992).

[17] N.B. Wilding, Phys. Rev. E **52**, 602 (1995).

[18] A.M. Ferrenberg and R.H. Swendsen, Phys. Rev. Lett. **61**, 2635 (1988); **63**, 1195 (1989).

[19] See, e.g., K. Binder, in *Computational Methods in Field Theory*, edited by H. Gausterer and C.B. Lang (Springer-Verlag, Berlin, 1992), pp. 59–125.

[20] T.A.L. Ziman, D.J. Amit, G. Grinstein, and C. Jayaprakash, Phys. Rev. B **25**, 319 (1982).

[21] R. Hilfer and N.B. Wilding, J. Phys. A **28**, L281 (1995).

[22] A.D. Bruce and N.B. Wilding, Phys. Rev. Lett. **68**, 193 (1992); N.B. Wilding and A.D. Bruce, J. Phys. Condens. Matter **4**, 3087 (1992).